J Mater Sci (2007) 42:8408–8417
DOI 10.1007/s10853-007-1787-3

Effect of surface modification of nanosilica on crystallization, thermal and mechanical properties of poly(vinylidene fluoride)

Rui Song · Debin Yang · Linghao He

Received: 22 December 2006 / Accepted: 18 April 2007 / Published online: 28 June 2007

Abstract Composites were prepared by solution blending ploy(vinylidene fluoride) (PVDF) and nanosilica which modified by different organic modifiers. Infrared analysis showed that the crystalline structure of PVDF was changed by the addition of RNS-A (silica with amino terminated group), while similar crystalline structure as pure PVDF was observed for composites with DNS-0 and DNS-2, unmodified silica and alkyl terminated group silica, respectively. With differential scanning calorimeter (DSC) and dynamic mechanic thermal analysis (DMTA) techniques, crystalline structure, thermal, and mechanical properties of the composite films were examined. As the DSC results showed, addition of SiO_2 would lead to the increased cooling crystallization temperature (T_c), implying that SiO_2 nanoparticles could act as nucleating agents, however the degree of crystallinity of PVDF was not elevated significantly. In the complementary modulated DSC curves, multi-melting peaks associated with non-reversing portion were observed and were explained from the viewpoint of melting-recrystallization in the DSC heating scan. In addition, dynamic mechanical properties as well as the thermal stability of the composites are also influenced by SiO_2. As manifested by the corresponding DMTA and thermogravimetric analysis (TGA) results, a strong interaction should exist between PVDF and SiO_2 nanoparticles.

R. Song (✉)
College of Materials and Chemical Engineering, Zhengzhou University of Light Industry, Zhengzhou 450003, China
e-mail: rsong@gucas.ac.cn

R. Song · D. Yang · L. He
College of Chemistry and Chemical Engineering, Graduate University of Chinese Academy of Sciences, Beijing 100039, China

D. Yang
e-mail: yangdebin2004@mail.china.com

L. He
e-mail: lhhe@zzuli.edu.cn

Introduction

Typical advantages of organic polymers are flexibility, toughness, formability, and low density [1]; whereas nanoparticles with their nanometer size, high surface area, and the associated performance of interfaces can be functioned as structure and morphology directors of the nanocomposites [2]. Incorporation of nanoparticles into various polymers to produce composites has been extensively utilized in an attempt to enhance the mechanical, physical, and thermal properties of polymer.

Poly(vinylidene fluoride) (PVDF) is a very attracting polymer owing to its piezoelectric [3] and pyroelectric characteristics [4] that have been exploited in the development of electronic devices [1, 5, 6]. It is known that PVDF can exist in three main crystalline modifications denoted as α (form II), β (form I), γ (form III). The α-phase has alternation trans- and gauche-bond (TGTG′), the β-phase has all trans-bond (TTTT), the γ-phase has a gauche-bond every fourth repeat unit (TTTGTTTG′) [7–9]. The IR spectra of these three crystalline phases have been well reported [9–17]: the characteristic α-phase are 530 cm^{-1} (CF_2 bending), 615 cm^{-1} and 765 cm^{-1} (CF_2 bending and skeletal bending), 796 cm^{-1} (CH_2 rocking), and 976 cm^{-1} (CH_2 twisting); the β-phase are 510 cm^{-1} (CF_2 bending) and 840 cm^{-1} (CH_2 twisting); the γ-phase are 512, 776, 812, 833, and 840 cm^{-1}.

The non-polar α-phase predominates at melting-crystallization below 160 °C while, the oriented polar β-phase is normally obtained by drawing of α-phase films between 70 °C and 100 °C. The un-oriented β-phase may be obtained by crystallization from dimethyl formamide (DMF) or dimethyl acetamide (DMAc) solutions at <70 °C and higher temperature will normally result in a mixture of the α and β-phase [13], with the α fraction increasing with temperature increase. The polar γ-phase may be obtained from both solution and melt-crystallization at temperature >160 °C, or by annealing α-phase samples between 175 °C and 185 °C [18–20].

In recent years some investigations had been done on the composite of PVDF/nanosilica system with main motivation to control the crystalline phase and therefore to confer the resulted material high mechanical and other properties [1, 2, 21]. Kim et al. employed the sol–gel process involving hydrolysis and polycondensation of TEOS (tetraethyl orthosilicate) to successfully prepare the PVDF/SiO_2 hybrid materials [1]. It was conclusively found that the PVDF/SiO_2 hybrid composite film of 5 wt% SiO_2 exhibited balanced mechanical properties without severe changes in the crystalline structure of PVDF; whereas for the hybrid composites with >10 wt% SiO_2, the films showed reduced mechanical properties and disrupted spherulite texture of PVDF in comparison with pure PVDF. Yet, some work showed that the presence of SiO_2 could increase toughness and/or stiffness through the energy-dissipation mechanism during deformation [22]. On the other hand, addition of appropriately surface-modified SiO_2 into PVDF can also control the crystalline phase and morphology of PVDF matrix, i.e., it is possible to obtain the specified crystalline phase in PVDF by changing the kind of surface modifier or the content of organically modified SiO_2 [2, 21].

In this study, through surface modification, SiO_2 nanoparticles with different terminated group were obtained and were then added into PVDF via solution blending to obtain the PVDF/SiO_2 composites, and the composite properties are investigated and compared with pure PVDF. The effects of surface modification of SiO_2 on the crystallization, thermal, and dynamic mechanical behavior of PVDF were further investigated.

Experimental

Materials and sample preparation

PVDF powders (F401, from Resin Corp. of Changzhou, China, with $M_n = 150 \times 10^3$, determined from the GPC measurement) was used as received. Silicon dioxide (SiO_2) with diameter about 20–30 nm was supplied by Henan University (Henan, China). The detail about the preparation of the surface-modification of nanosilica could be found elsewhere [23, 24]. Briefly, a polyreaction-like process where the hydrolysis product of sodium metasilicate is used as the monomer and hexamethyldisilazane (HMDS) as the chain terminator. As received, the silica with two different substituted end group were prepared via surface modification and the surface groups in this case were following: long chain alkyl, long chain alkylamine, and amino group. Dimethylformamide (DMF, purity of 99.5%) was from Tianjin Chemical Reagent Company (Tianjin, China). All other raw materials were used as received.

At room temperature PVDF and SiO_2 were dissolved in DMF (weight ratio of SiO_2/PVDF = 3 wt% and PVDF/DMF = 10 wt%, respectively) by stirring for about 2 h, followed by sonicating for 1 h before quickly poured into a self-made aluminum cell. Finally the resultants were annealed under vacuum at 70 °C for one week to form a homogeneous film of ca. 0.4 mm thickness (sample I). In this case, the annealing process was used to remove the solvent and spontaneously induce the crystallization of PVDF. To obtain more insight on crystallization behavior, sample I was quickly heated to 200 °C, which was above the melting temperature of PVDF, and then keeping the sample at 200 °C for 2 min to remove any traces of crystalline structure; finally the sample was cooled down to 30 °C at a cooling rate of 10 °C/min to obtain the melt-crystallized sample (sample II).

For samples with 3 wt% SiO_2/PVDF the shorthand notations were used in the following text: the bare silica and the silica with surface modified with amino and alkyl groups were nominated DNS-0, RNS-A, and DNS-2, respectively.

Characterization and measurement

Attenuated total reflection (ATR)-infrared spectra were obtained using a FT-IR spectrophotometer (Bruker, Tensor 27), at the resolution of 4 cm^{-1}, 32 scans. In ATR mode, thick sample can be directly tested by collection the reflection information of single infrared beam on the sample surface. As one of the advantages, the ATR-IR allows easy investigation of thick sample in the practical condition, without tedious treatment for sample.

Based on the specific absorption bands of α- and β-phase, a method had been introduced elsewhere was used to calculate the fraction of β-phase [18]. By using two adsorption bands at 763 cm^{-1} and 840 cm^{-1} that are characteristic to α and β-phase, respectively, the fraction of β-phase, F(β), can be calculated using the following equation [25]:

Table 1 F(β) values of samples annealed at 70 °C for 1 week (sample I), ($F(\beta)_I$) and that of melt-crystallized (sample II), $F(\beta)_{II}$

Sample	Neat PVDF (%)	DNS-0 (%)	DNS-2 (%)	RNS-A (%)
$F(\beta)_I$	54.4	71.5	74.5	24.9
$F(\beta)_{II}$	4.3	4.8	7.9	7.8

$$F(\beta) = A_\beta/(1.26A_\alpha + A_\beta) \quad (1)$$

where A_α and A_β were the absorbencies of α and β-phase at 763 cm^{-1} and 840 cm^{-1}, respectively and the F(β) values derived from the IR test were listed in Table 1. In this case, Eq. 1 was used as a measurement of the transformation efficiency of gauche state to all-trans state in PVDF film.

For DSC measurement, all samples were analyzed by Q100 temperature modulated DSC from TA Corporation which equipped with the thermal analysis data system. Prior to sample scan, the heat flow and temperature were calibrated with sapphire and pure indium (In), respectively, and two standard empty aluminum pans were used for baseline calibration. Under nitrogen atmosphere (20 mL/min), the samples were scan over the range of 0–200 °C at a heating rate of 10 °C/min for conventional DSC. In the modulated DSC mode, nitrogen flow: 25 mL/min (increasing nitrogen flow was to prevent the sample from oxidizing at slowly heating rate), heating rate: 3 °C/min, amplitude: ±1 °C and 60 s period were adapted for the samples scan.

To derive the information of sample crystallinity from the DSC results, the degree of mass crystallinity (χ_c^d) was calculated as follows:

$$\chi_c^d = (\Delta H_m)/w(\Delta H_m^0) \times 100\,\% \quad (2)$$

where ΔH_m was the experimental enthalpy of fusion and w was the PVDF content in the PVDF/SiO_2 composites. In this case, a value of 104.6 J/g was used for ΔH_m^0 as the heat of fusion of 100% crystalline PVDF [26, 27].

Crystalline morphologies were recorded using Nikon Eclipse E600 polarized optical microscope (POM). During the sample testing process, the applied magnification was used to obtain a well-resolved image, so the magnification was not fixed for different samples. The photographs for the sample films were taken with a Nikon Coolpix 5600 digital camera equipped on the vertical hood of the optical microscope.

Dynamic mechanic thermal analysis (DMTA) experiments were performed in film tension mode with a TA instruments Q800 DMTA device at a heating rate of 3 °C/min from 30 °C to 155 °C, frequency of 1 Hz. The sample dimension was $30 \times 5 \times 0.4$ mm^3. Thermogravimetric analysis (TGA) was performed on a STA 409 PC, manufactured by Netzsch GmbH, Germany. The sample was heated from room temperature to 600 °C at a heating rate of 10 °C/min under a constant flow of nitrogen gas.

Results and discussion

ATR-IR and POM results

As stated in the experimental part, two series of crystallized samples were used through the investigation: one was the composite films annealed at 70 °C for one week (sample I) and the other was from the melting state (sample II). They were prepared to highlight the discrepancy in the crystallinity behavior, which generated by different procedure. The ATR-IR results and the related POM images from the samples of solution crystallization are showed in Fig. 1. In Fig. 1a, sharp α-characteristic peaks at 764 cm^{-1}, 976 cm^{-1} can be observed for RNS-A system; whereas strong β-characteristic (840 cm^{-1}) can be seen for neat PVDF, DNS-0, and DNS-2 systems.

With Eq. 1 the β contents for both series ($F(\beta)_I$, $F(\beta)_{II}$ for sample I and sample II, respectively) could be derived and the results are illustrated in Table 1. As indicated, RNS-A system has the lower $F(\beta)_I$ value (24.9%), which implies the dominant α-phase; whereas the higher $F(\beta)_I$ values (71.5%, 74.5% for DNS-0 and DNS-2, respectively) of the samples filled with DNS-0 and DNS-2 silica display the predominant β-phase. For neat PVDF, the lower $F(\beta)_I$ value of 54.4% than that of DNS-0 and DNS-2 systems, implies the comparable α-phase and β-phase in neat PVDF. In conclusion, for sample I, the addition of DNS-2 and DNS-0 silica could promote the β-phase, while more α-phase will be generated in the presence of RNS-A silica.

In addition, from the result of POM observations of neat PVDF, DNS-0, and DNS-2 systems (β-dominated sample), we can find many small spherulites belonging to the β crystalline phase, but similar feature could not be found from the POM image of RNS-A system (see Fig. 1b). For RNS-A system, the imperfect crystalline particles should be ascribed to the spherulite of α crystalline phase and it will be able to develop into large spherulite upon annealing at higher temperatures (results not showed).

In comparison, the observation is very different from the sample via melting-crystallization process (sample II), as showed in the corresponding FTIR and POM results (Fig. 2). Although α and β are still the main crystalline phase (see Fig. 2a), for all samples lower $F(\beta)_{II}$ values can be found in Table 1. Therefore the samples should have the dominated α-phase. This is in agreement with other previous work indicated that during the melt-crystallization process, the PVDF is more tend to form the non-polar α-phase and polar γ-phase [28]. In this case, no obvious γ-phase is emerged, though.

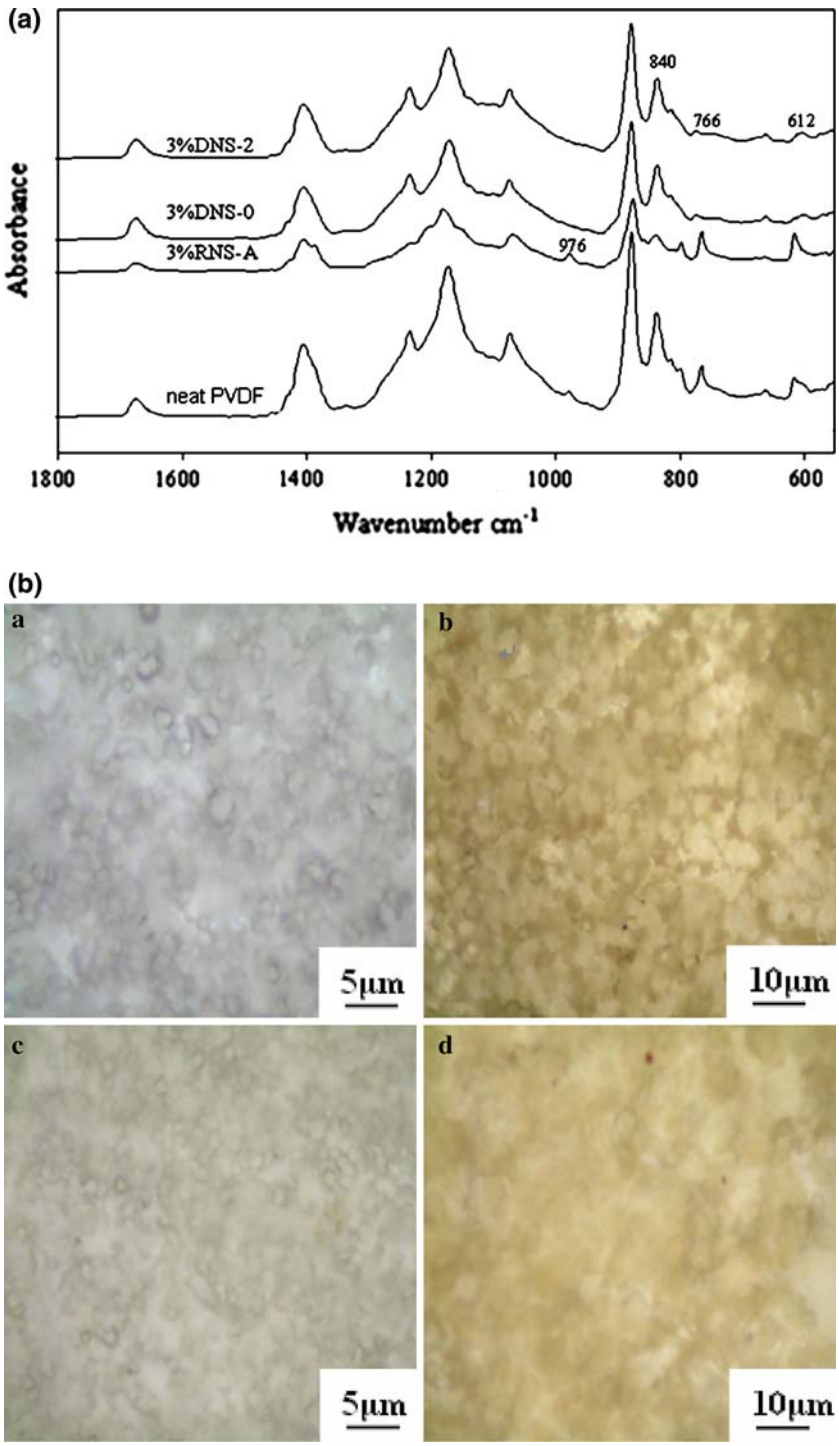

Fig. 1 FT-IR spectra of sample I (**a**) and polarized light macroscopic images of sample I (**b**), a: neat PVDF, b: DNS-0, c: DNS-2, d: RNS-A

Meanwhile, tremendous difference among all the samples can be found from the POM results in Fig. 2b. Although the four systems show the spherulite structure which is indicative of the dominant α-phase, the variance in the spherulite size are clearly revealed, i.e., neat PVDF > DNS-0 ~ DNS-2 > RNS-A.

With the addition of silica nanoparticle, a lowered spherulite size is obviously observed, and this observation is more distinct in particular for the sample filled with RNS-A, which suggests that the dispersed SiO_2 particles in the hybrid composite would disturb the crystal growth of PVDF component. As noted, the spherulite of the sample via melting-crystallization (sample II) is significantly larger in size and more perfect than that of the annealed-induced (sample I), which is the reason why relatively large spherulite size normally means a higher content of α-phase (Table 1).

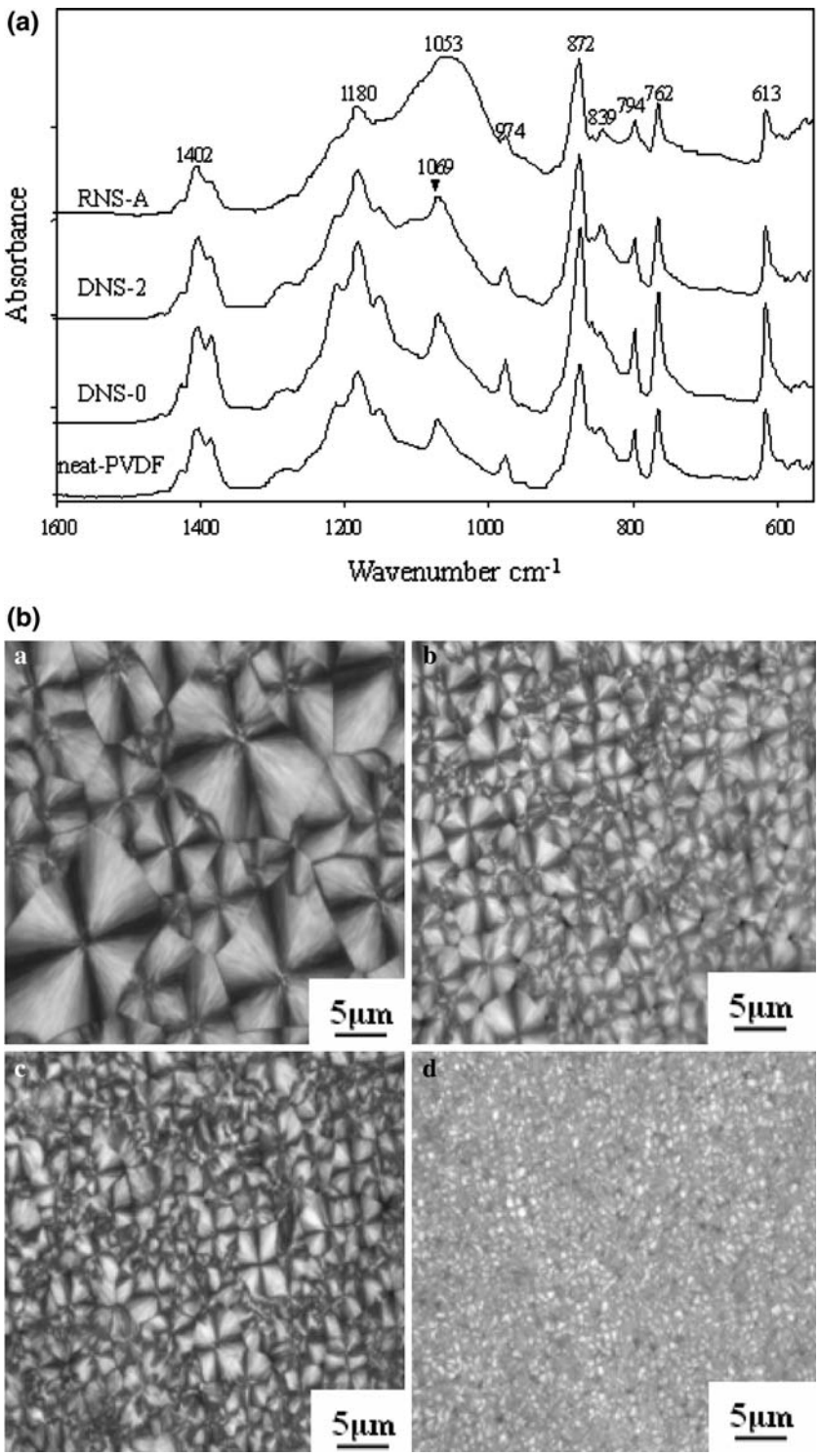

Fig. 2 FT-IR spectra of sample II (**a**) and polarized light macroscopic images of sample II (**b**), a: neat PVDF, b: DNS-0, c: DNS-2, d: RNS-A

DSC and MDSC measurement

DSC scans, including the heating and the cooling of the samples from 70 °C-annealed (sample I) are showed in Fig. 3. For RNS-A system with predominant α-phase PVDF, we can find the main melting peak at ca. 163 °C and a very weak shoulder peak at ca. 159 °C. As to the β-phase predominant samples (neat PVDF, DNS-0, and DNS-2 systems), only single melting peak occurred at ca. 161–164 °C.

Comparing with the pure PVDF, an elevating crystallization temperature (T_c) can be found in the cooling scan for

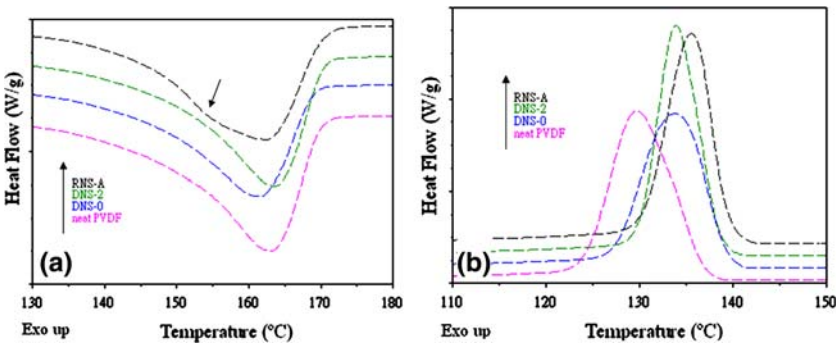

Fig. 3 DSC traces of sample I; (**a**) heating curves; (**b**) cooling curves

all the composites, DNS-0 at ca. 134 °C, DNS-2 at ca. 134 °C, and RNS-A at ca. 136 °C, respectively. These elevating T_c temperatures often imply the accelerating crystallization rate due to the nucleating effect from the incorporation of nanosilica [29]. In this case, this phenomena is more apparent for all composites considering the fact that pure PVDF with T_c about 130 °C, and this is particularly true for RNS-A system which with T_c about 136 °C.

The peak temperature in the heating scan (T_m) and areas of the endotherm (ΔH_f^c) are listed in Table 2. The mass fraction degrees of crystallinity (χ_c^d) are determined from the related endotherm area and are tabulated in the last column of Table 2. From the results of χ_c^d data, the lower χ_c^d value (31.5%) for DNS-0 system than that of neat PVDF (36.5%) seems contradictory with the result of T_c, and this observation should be ascribed to the non-modified DNS-0 silica which is very hydrophilic and bears higher surface energy. During the crystallization, this polar and hydrophilic nanoparticle will tend to surround the PVDF's segments and hence restrict the mobility of molecular chains and thus retard the crystallization [29, 30]. As comparison, both DNS-2 and RNS-A systems have similar χ_c^d values with neat PVDF, and this can be explained by the decreasing surface energy and adsorption effect of organically modified DNS-2 and RNS-A.

Table 2 Related data from DSC measurement of samples: crystalline temperature (T_c), melting temperature (T_m), heat of fusion (ΔH_f^c), mass fraction crystallinity (χ_c^d)

	Neat PVDF	DNS-0	DNS-2	RNS-A
Sample I				
T_c (°C)	130	134	134	136
T_m (°C)	163	162	164	163
ΔH_f^c (J/g)	38.23	31.96	37.06	37.71
χ_c^d (%)	36.5	31.5	36.5	37.2
Sample II				
T_c (°C)	130	133	132	132
T_m (°C)	164	165	165	165
ΔH_f^c (J/g)	38.77	36.20	37.28	35.68
χ_c^d (%)	38.2	35.7	36.7	35.2

Compared with sample I, ΔH_f^c and χ_c^d values for sample II are not altered largely (not presented), but a narrowed melting peak and a slightly elevating T_m (ca. 165 °C, see Fig. 4) could be found, which implying the formation of more perfect and stable crystal during the melting process and this observation is also consistent with above POM results (Fig. 2b). In addition, for all samples except for pure PVDF, shoulder peak could not be found around the main melting area, which is different from the shoulder peak occurred for RNS-A system in sample I.

Another noteworthy aspect during the melting process of samples is the multi-melting phenomenon, which has been observed in the DSC curves for many semi-crystalline polymer, and has been attracted a variety of investigations in theoretical and experimental [31–36]. The possible

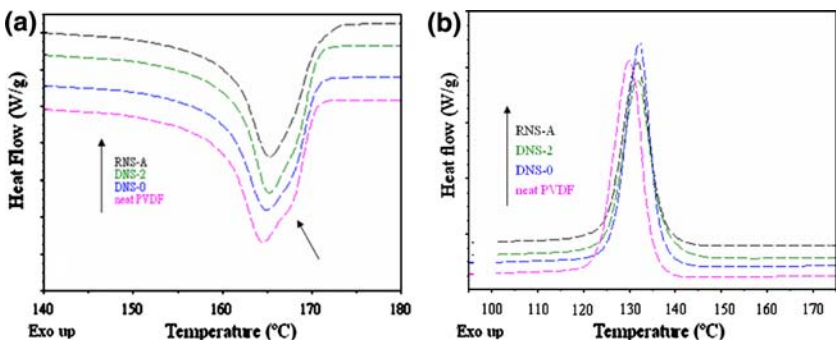

Fig. 4 DSC heating traces of sample II, (**a**) heating curves; (**b**) cooling curves

origin of this phenomena may be ascribed to (1) melting, re-crystallization, and re-melting during the DSC heating process; (2) the presence of more than crystal modification (polymorphism); (3) variation in morphology (such as lamellar thickness, distribution, perfection, or stability); (4) physical aging or/and relaxation of the rigid amorphous fraction; (5) different molecular weight species and so on [37]. Modulated DSC (MDSC) applies a sinusoidal temperature oscillation on a linear heating/cooling conventional DSC and makes the total heat flow to be separated into the heat capacity-related (reversible) and kinetic (non-reversible) components. In order to further study the melting behavior of samples, this technique is performed and the corresponding curves are showed in Figs. 5 and 6.

At first look, the T_m values determined from the MDSC total heat flow, normally located at ca. 170 °C, were higher than those from the conventional DSC. This is reasonable in that with relatively low scan rate with MDSC, 3 °C/min in this case, the time duration was long enough for the crystallite to be more perfect. In Addition, comparing them with related conventional DSC curves, several aspects should be underlined upon close check the MDSC results. First, the multi-melting peaking phenomenon of sample II is more evident and complicate than the counterpart sample I. Further, as we check the total heat flow in Figs. 5 and 6, we can find that for α-phase dominated sample II, two apparent T_m appear with the main peak located at ca. 165 °C and the other at ca. 170 °C as the shoulder peak. By comparison, for sample I only one well-resolved T_m appears at ca. 170 °C but the shoulder peak is very weak. This observation suggests sample II has a higher level of crystal perfection than the sample I [38], and this respect could be evidenced more directly from the OM images in Figs. 1b and 2b.

Second, upon comparing the non-reversible heat flow curves, for I series only RNS-A composite indicated the re-crystallization which revealed as one hump cover the temperature ranging from ca. 135 °C to 160 °C (see the RNS-A exotherm in Fig. 5c). While all composites of Π series, irrespective of the variation of the silica surface modification, displayed the similar behavior (see the non-reversible curves marked in the square box in Fig. 6c). Moreover, sample I shows the well-separated double melting peaks, while all composites of II series display varied, multi-melting peaks.

Finally, upon further checking the reversing heat flow of two series of samples, the discrepancy could be seen with respect to the variation of T_m. For I series, the samples have the decreased T_m values in the range of ca. 168~164 °C in the following order: neat PVDF, DNS-0, DNS-2, and RNS-A (see Fig. 5b). In comparison, the Π series has the almost constant T_m value at approximate 164 °C (see Fig. 6b). This observation is acceptable considering two facts. First,

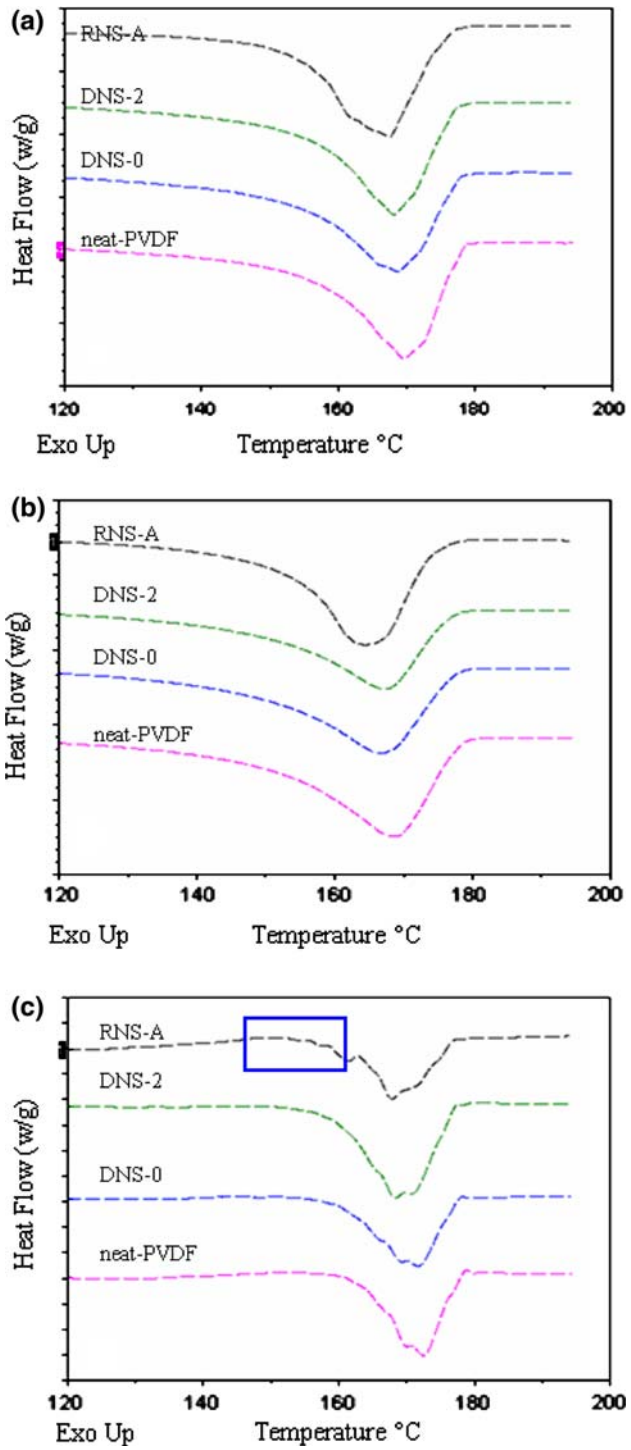

Fig. 5 TMDSC heat flow traces of sample I. (**a**) Total heat flow, (**b**) reversing heat flow, (**c**) non-reversing heat flow. The box on the curve indicated the temperature range concerning the re-crystallization

for sample II which are subjected to 200 °C for 2 min prior to cooling down to room temperature, the influence from the surface modified silica particles could be excluded, thus this series have a constant T_m; on the contrary, the silica particles should play a role during the crystallization of

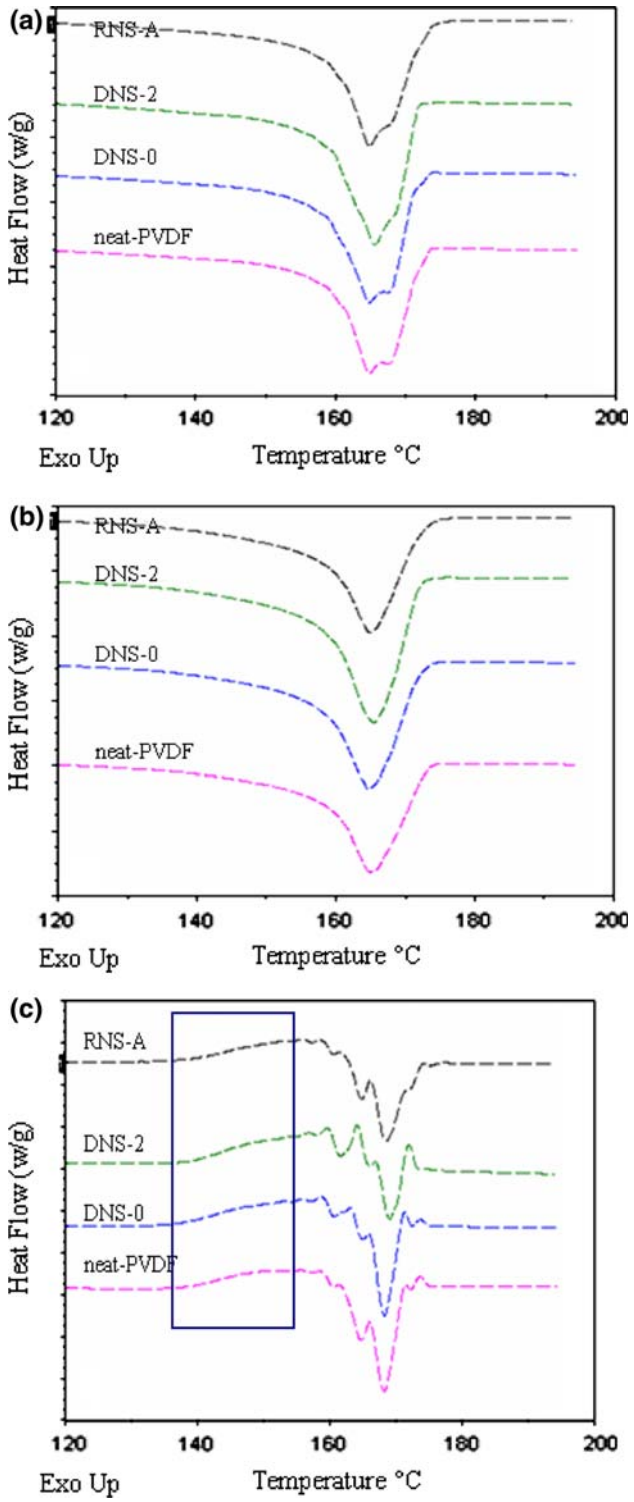

Fig. 6 TMDSC heat flow traces of sample II. (**a**) Total heat flow, (**b**) reversing heat flow, (**c**) non-reversing heat flow. The box on the curves indicated the temperature range concerning the re-crystallization

sample I which had been annealed at 70 °C for 6 days. In other words, the silica could act as the nucleator in the subsequent crystallization step. Second, this observation is also in well agreement with the IR result summarized in Table 1, i.e., all samples in series II have a relatively low β contents with $F(\beta)_{II}$ less than 10%; whereas the sample I have increased β contents $F(\beta)_I$ from 24.9% to 74.5% which will lead to the elevated T_m values.

Thermal stability

The thermal stability is evaluated with TGA measurement and the results are presented in Fig. 7. In this case, both series of samples display the very identical results and to avoid encumbrance only the results of sample I are given. Comparing with the pure PVDF, the composites comprised of the DNS-0 and RNS-A silica are more thermal-stable but no enhancement is found for the DNS-2 system. It means that the nanocomposites comprised of the polar group-modified silica exhibit better thermal stability than that of pure PVDF and the non-polar group-modified silica composite. Due to the well dispersion and good thermal transmission properties, the silica nanoparticles may strongly hinder the volatility of the decomposed products obtained from pyrolysis and thus limit the continuous decomposition of PVDF content. In addition, as we discussed above, the restrained state of PVDF chains due to the interaction between the chains and the polar groups on the silica surface, i.e., amino and/or hydroxyl in this case, is another important factor to induce an enhancement of thermal stability of the nanocomposites.

DMTA measurement

DMTA measurements are employed to get further information on the dynamic behavior of the composites and temperature dependence of E′ (storage modulus) and tanδ

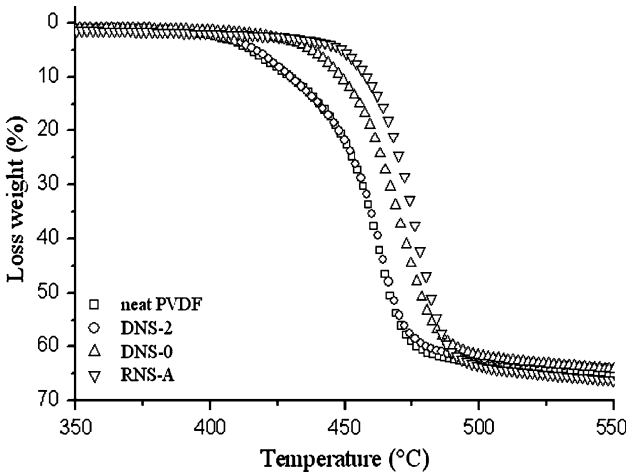

Fig. 7 TGA curves for neat PVDF and different PVDF/SiO_2 nanocomposites of sample I

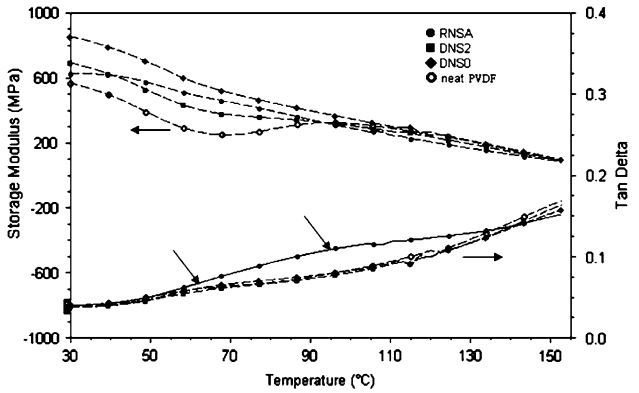

Fig. 8 Temperature dependence of storage modulus and tanδ of sample I

(loss factor) are showed in Fig. 8. As expected, E′ of these composites are higher than that of neat PVDF and decrease with elevating temperature for all samples. Here, the E′ of DNS-0 series is much higher than others. The elevating E′ suggests, apart from the physical enhancement from the inorganic particle to the polymer matrix, certain interaction may exist in between the chemically modified nanoparticles and PVDF segments, which may prevent the motion of PVDF chains. In this case, higher E′ of DNS-0 implies the stronger interaction of unmodified nanoparticles (with plenty of hydroxyl groups on the silica) with PVDF matrix than the organically modified ones, and this aspect could be also corroborated with the lower χ_c^d data listed in Table 2.

Another noteworthy point is, above ca. 50 °C, one weak relaxation process emerges in the tanδ (loss factor) curves. This process, normally labeled α_c, is closely associated with the motions within the crystalline fraction and is resulted from the *higher-T_g-relaxation* which had been also reported in a variety of flexible semi-crystalline polymers, including polyethylene, poly(methylene oxide), poly(ethylene oxide) and isotactic polypropylene [39, 40]. It should be noted that this relaxation is not clearly revealed as a peak in the tanδ plot, and this observation should be ascribed to the small size of the spherulite (see Fig. 1b) and lower crystallinity (see Table 2 for the relatively low χ_c^d of sample I) that are induced by the 70 °C-annealing process.

For RNS-A composite, the higher α_c transition temperatures imply the strong interaction of RNS-A with PVDF chains as corroborated well in the DSC and TGA measurements; and the large tanδ value corresponding to the α_c transition region in the DMTA curve is probably due to the imperfect crystalline structure that induced by RNS-A in the increasing volume of continuous crystalline region and the scattering amorphous region. This interpretation can be also employed to explain the results of F(β) data in Table 1. The strong interaction of RNS-A with PVDF chains would increase the motion resistance of PVDF chains and this effect will make it more difficult to form the *all-trans* conformation (β-phase) for the molecular chain and thus it tends to form the alternating *trans* and *gauche* state (α-phase). Accordingly, the relatively weak interaction of DNS-2 with PVDF chains implies the easy motion of PVDF chains as that in the neat PVDF, hence all-trans β-phase can be formed. Although this explanation deserves further studies, these experimental results highlight the potential to control the crystalline phase and thus endow the composite with high mechanical and other properties.

Conclusion

In this investigation, surface modified silica via different chemical groups are incorporated into PVDF to form the PVDF/SiO_2 composites. ATR-IR measurements and the corresponding POM results indicated the crystalline phase of PVDF is alternated by the addition of SiO_2. For DNS-0 and DNS-2 systems, the predominant crystalline phase is β-phase as neat PVDF; for RNS-A series, α-phase is the main crystalline phase. From the DSC measurement, the double-melting peak phenomena is present for RNS-A system, and the crystalline temperature (T_c) of PVDF is elevated with the addition of SiO_2, indicating that the SiO_2 particles would act as nucleating agents to accelerate the crystallization of PVDF. Temperature modulated DSC (MDSC) experiments are performed to better understand the melting behavior nanocomposites and the results verify that the multi-melting contributions are associated with the non-reversing portion of the MDSC measurement. In addition, DMTA and TGA results show improved dynamic mechanical properties and thermal stability for the nanocomposites.

Acknowledgment We are grateful to Prof. Zhijun Zhang from the Henan University for supplying the silica nanoparticle in this research. This work was partially subsidized by Henan Innovation Project for University Prominent Research Talents (''HAIPURT'') program.

References

1. Kim JW, Cho WJ, Ha CS (2002) J Polym Sci: Part B: Polym Phys 40:19
2. Shah D, Maiti P, Gunn E, Schmidt DF, Jiang DD, Batt CA, Giannelis EP (2004) Adv Mater 16:1173
3. Greschke D, Leister N, Steffen M, Glasel HJ, Hartmann E (1997) J Mater Sci Lett 16:1943
4. Bergman JG, Mcfee JH, Grane GR (1971) Appl Phys Lett 18:203
5. Mironi-Harpaz I, Narkis M (2001) Polym Eng Sci 41:205
6. Lu FJ, Hsu SL (1986) Macromolecules 19:326
7. Hasegaua R, Kobayashi M, Tadokoro H (1972) Polym J 3:591
8. Bachmann MA, Gordon WL, Koenig JL, Lando JB (1979) J Appl Phys 50:6106

9. Benedetti E, Catanorchi S, D'Alessio A, Moggi G, Vergamini P, Pracella M, Ciardelli F (1996) Polym Int 41:35
10. Davis GT, McKinney JE, Broadhurst MG, Roth SC (1978) J Appl Phys 49:4998
11. Hsu SL, Lu FJ, Waldman DA, Muthukumar M (1985) Macromolecules 18:2583
12. Benz M, Euler WB (2003) J Appl Polym Sci 89:1093
13. Gregorio Jr R, Cestari M, (1994) J Polym Sci: Part B: Polym Phys 32:859
14. Tashiro K, Kobayashi M, Tadokoro H (1981) Macromolecules 14:1757
15. Kobayashi M, Tashiro K, Tadokoro H (1975) Macromolecules 8:158
16. Peng Y, Wu P (2004) Polymer 45:5295
17. Gregorio R (2006) J Appl Polym Sci 100:3272
18. Salimi A, Yousefi AA (2003) Polym Test 22:699
19. Bocaccio T, Bottino A, Capanelli G, Piaggio P (2003) J Membr Sci 210:315
20. Bormashenko Y, Pogreb R, Stanevsky O, Bormashenko E (2004) Polym Test 23:791
21. Buckley J, Cebe P, Cherdack D, Grawford J, Seyhan B, Jenkins M, Pan J, Reveley M, Washington N, Wolchover N (2006) Polymer 47:2411
22. Yang D, Bei W (1994) Proceedings of the IEEE International Symposium on Electrical Insulation, Pittsburgh, PA, June 5–8, 1994, p 590
23. Li X, Cao Z, Liu F, Zhang Z, Dang H (2006) Chem Lett 35:177
24. Zhang ZJ, Zhang J, Xue QJ (1994) J Phys Chem 98:12973
25. Salimi A, Yousefi AA (2004) J Polym Sci: Part B: Polym Phys 42:3487
26. Rosemberg Y, Sigmann A, Narkis M, Shkolnik S (1991) J Appl Polym Sci 43:535
27. Marega C, Marigo A (2003) Eur Polym J 39:1713
28. Sajkiewicz P (1999) Eur Polym J 35:1581
29. Joziorny A (1978) Polymer 19:1142
30. Chen MJ, Tian G, Zhang Y, Wan C, Zhang Y (2006) J Appl Polym Sci 100:1889
31. Pyda M, Wunderlich B (2000) J Polym Sci Polym Phys 38:622
32. Pak J, Wunderlich B (2001) Macromolecules 34:4492
33. Okazaki I, Wunderlich B (1997) Macromolecules 30:1758
34. Hu W, Albrect T, Strobl G (1999) Macromolecules 32:7548
35. Albrecht T, Armbruster S, Keller S, Strobl G (2001) Macromolecules 34:8456
36. Schick C, Wurm A, Mohamed A (2002) Thermochim Acta 392:303
37. Liu T, Petermann J (2001) Polymer 42:6453
38. Prest WM, Luca D (1975) J Appl Phys 46:4136
39. Mano JF, Sencada V, Costa AM, Lanceros-Méndez S (2004) Mater Sci Eng A 370:336
40. Boyd RH (1985) Polymer 26:323